Transition metal sulfide hydrogen evolution catalysts for hydrobromic acid electrolysis

Supplementary Information

Anna Ivanovskaya, [1a] *Nirala Singh,* [2] *Ru-Fen Liu,* [1] *Haley Kreutzer,* [3] *Jonas Baltrusaitis,* [4] *Trung Van Nguyen,* [3] *Horia Metiu,* [1] *Eric McFarland*[21]

[1]Department of Chemistry and Biochemistry, University of California, Santa Barbara, California 93106

[2] Department of Chemical Engineering, University of California, Santa Barbara, California 93106

[3]Department of Chemical & Petroleum Engineering, The University of Kansas, Lawrence, Kansas 66045

[4]PhotoCatalytic Synthesis Group, MESA+ Institute for Nanotechnology, Faculty of Science and Technology, University of Twente, Meander 225, P.O. Box 217, 7500 AE Enschede, The Netherlands

[a] To whom correspondence should be addressed: annai@seamedical.com, Phone: 805-729-3274; ewmcfar@engineering.ucsb.edu, Phone: 805-893 4343, Fax: 805-893 4731

1) Experimental supplementary information:

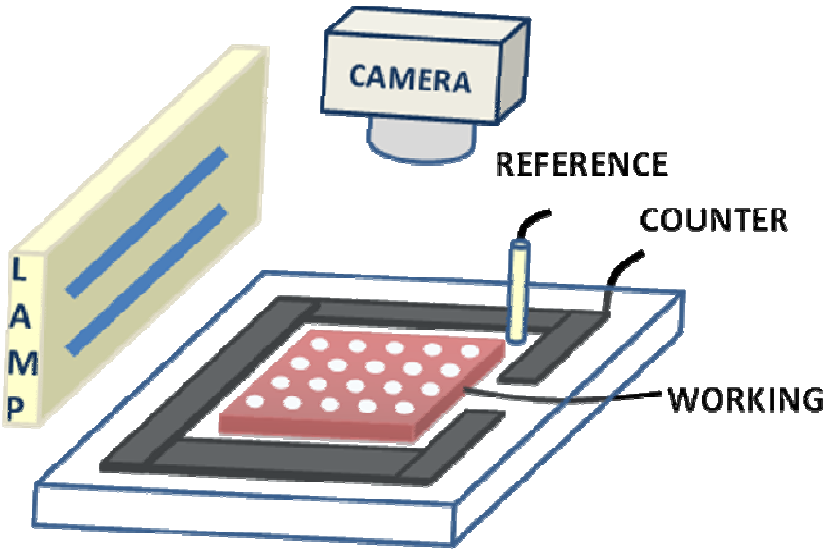

Figure S1. Schematic of electrochemical high-throughput screening system. Electroreduction of HBr, performed on TMS samples in parallel, is monitored by observing hydrogen bubbles evolved during cyclic voltammetry.

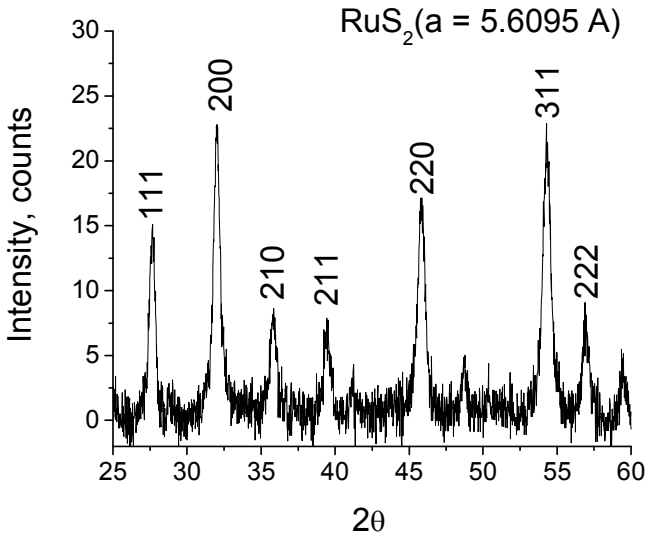

Figure S2. X-Ray Diffraction Spectrum of RuS_2

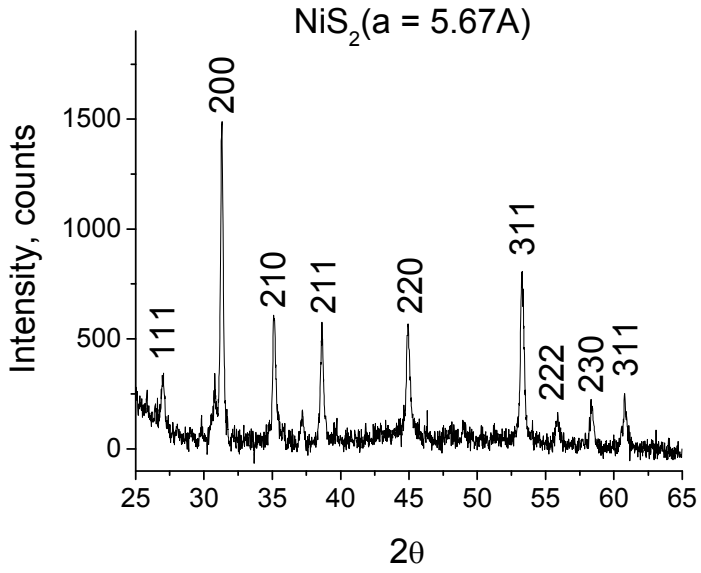

Figure S3. X-Ray Diffraction Spectrum of NiS_2

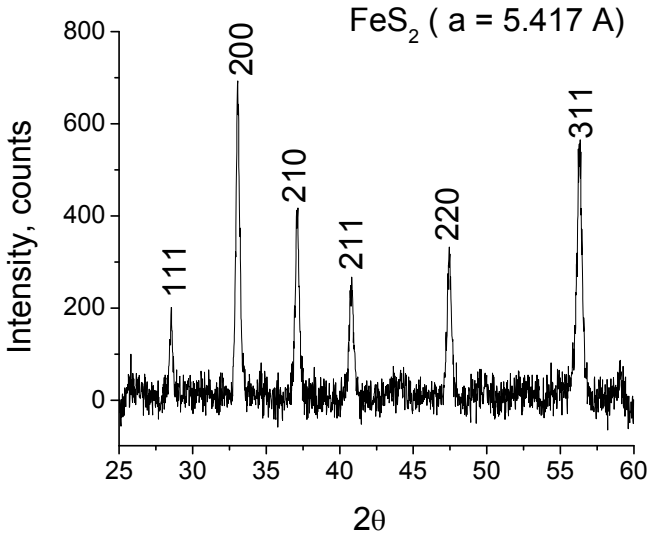

Figure S4. X-Ray Diffraction Spectrum of FeS_2

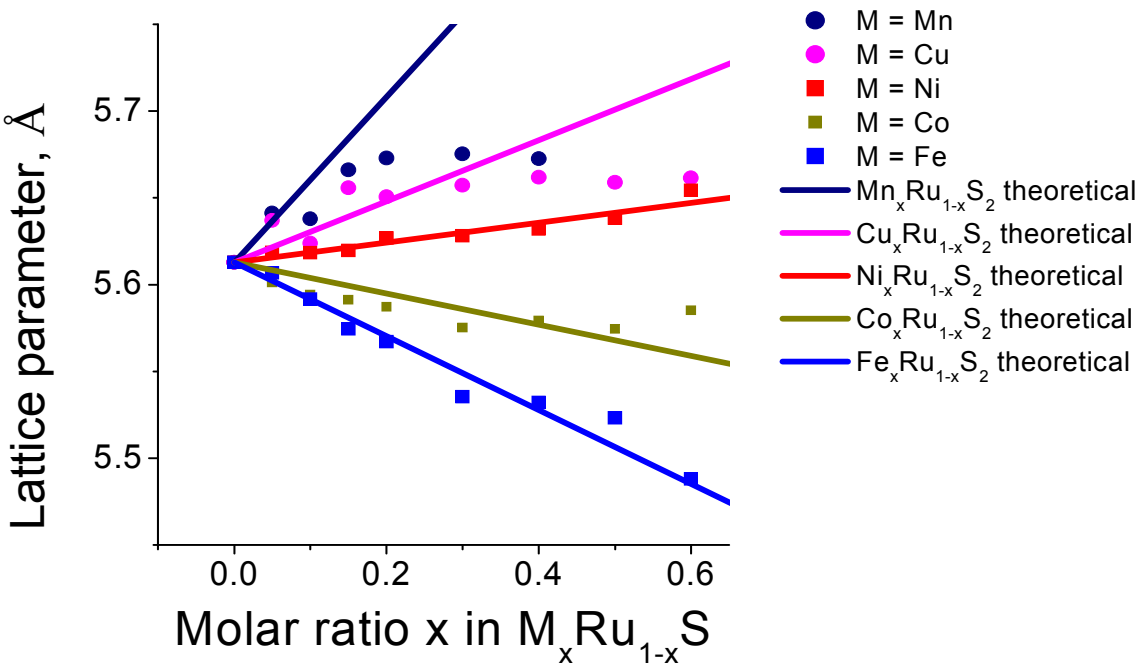

Figure S5. Lattice parameters of substituted RuS_2 pyrite structure, derived from X-ray diffraction peak positions (measured values shown as points), and theoretical lattice parameters as calculated using Vegard's Law (shown as solid straight lines).

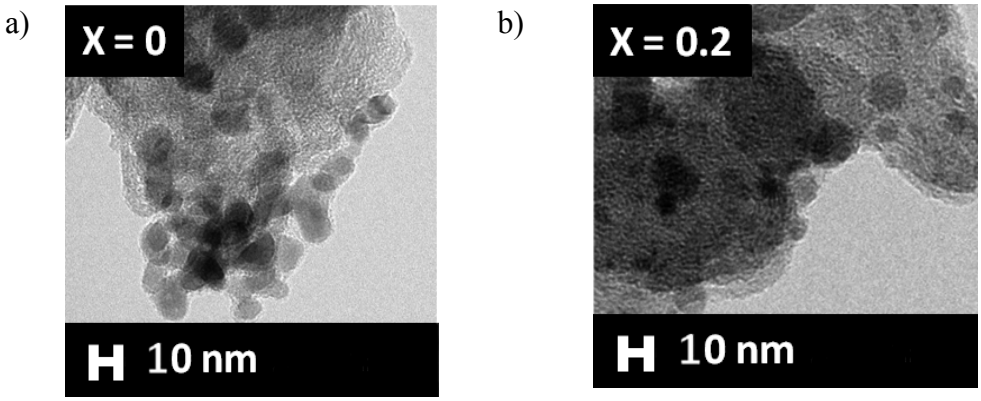

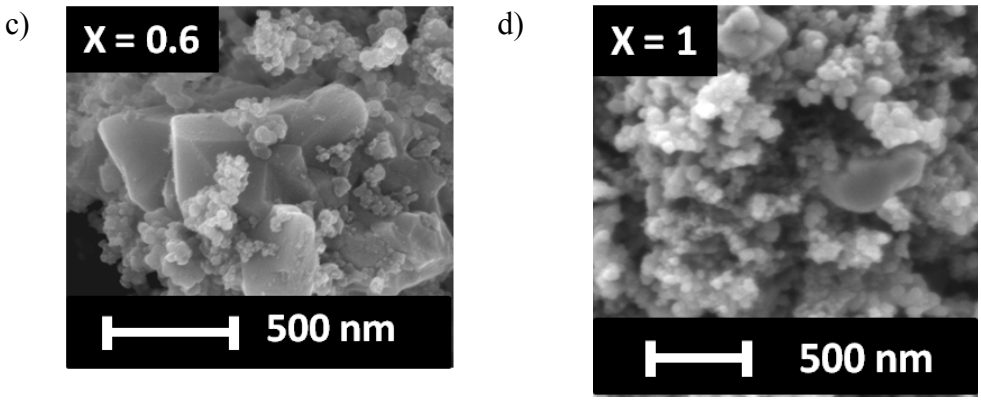

Figure S6. Morphology of Co-substituted RuS_2 as a function of substituted metal molar fraction (X). a) TEM of RuS_2 (pyrite) nanoparticles; b) TEM of $Co_{0.2}Ru_{0.8}S_2$ (mixed pyrite phase); c) SEM of Co_9S_8 (pentlandite) submicron particles; d) SEM of CoS_2 (pyrite) submicron particles.

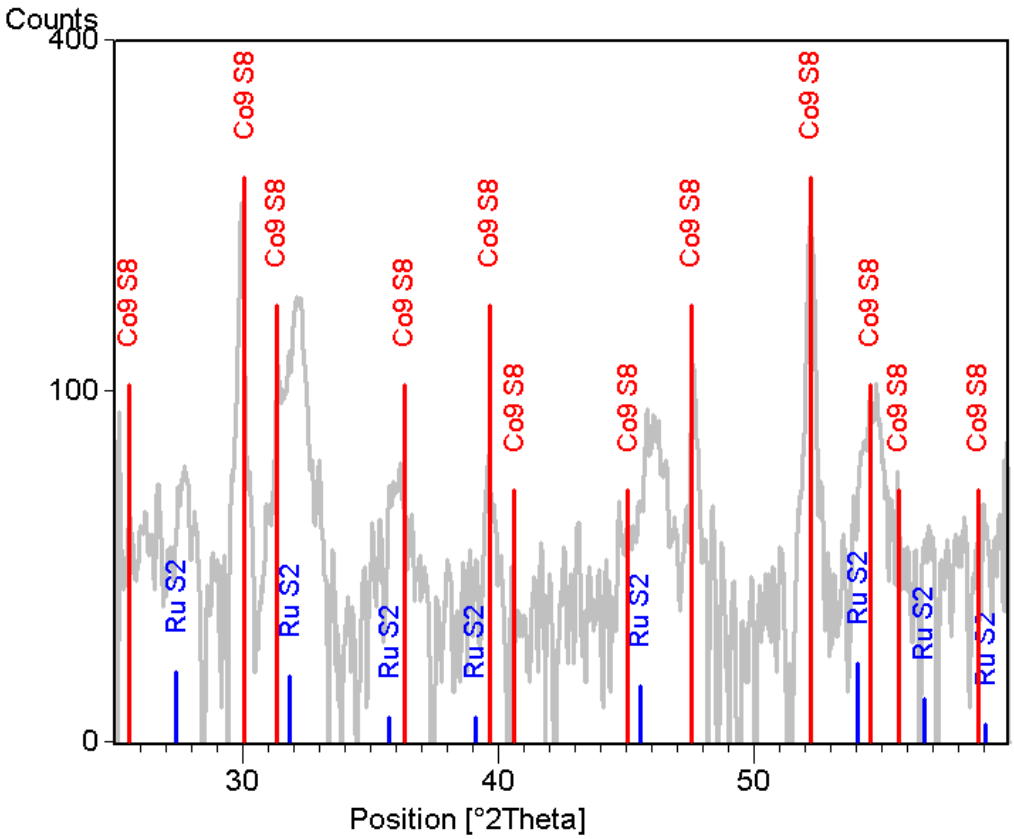

Figure S7. X-Ray Diffraction Spectrum of Co substituted RuS_2 (Co:Ru = 0.6:0.4)

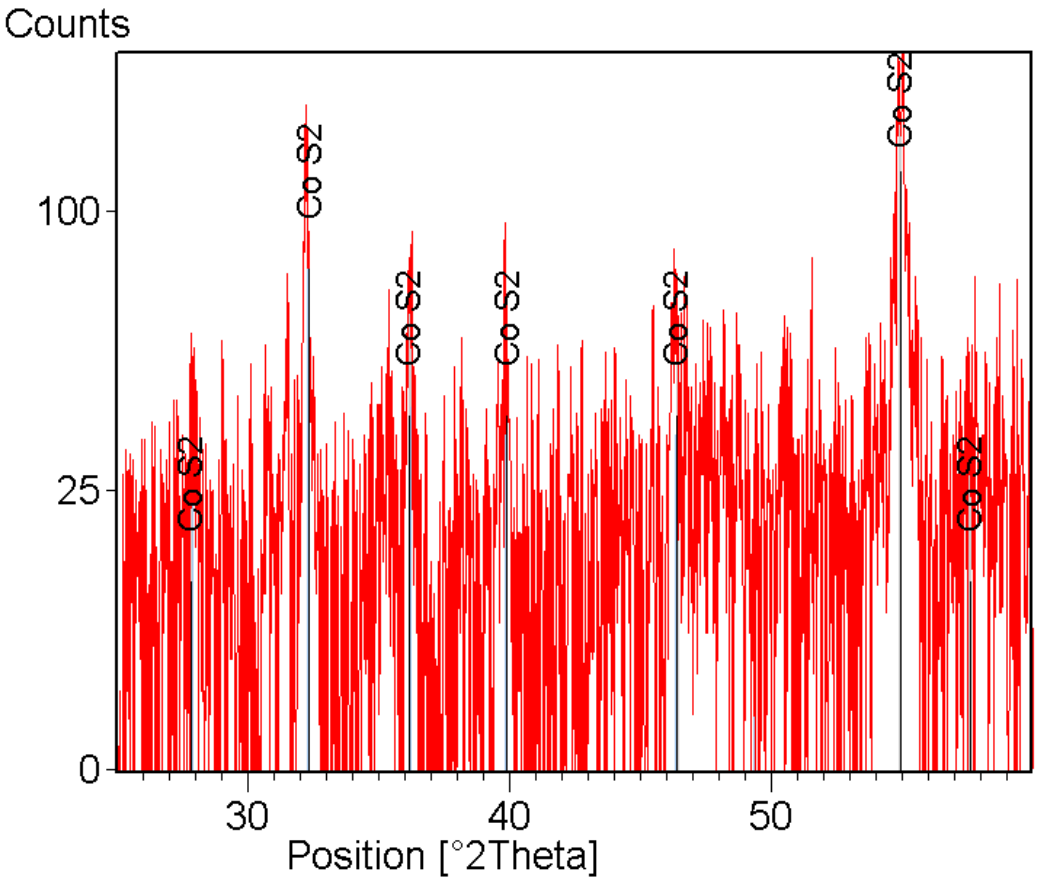

Figure S8. X-Ray Diffraction Spectrum of cobalt sulfide

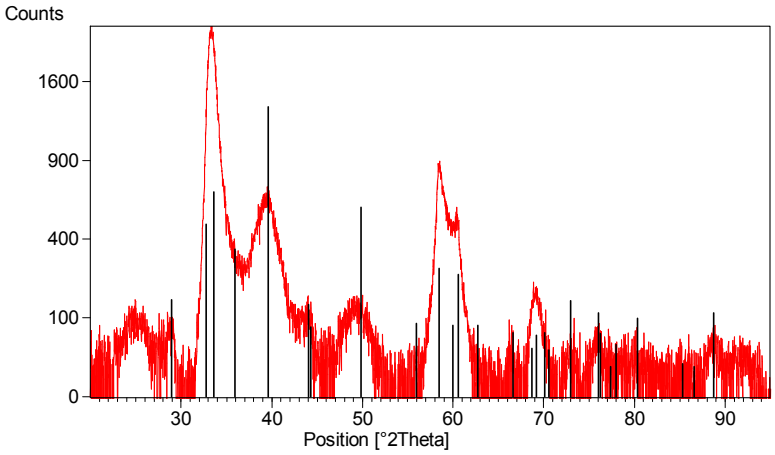

Figure S9. X-Ray Diffraction Spectrum of WS_2

Synthesis of TMS with hexagonal structure

Mo and W sulfides were synthesized first as dioxides, which are further reacted in H_2S to form disulfides.

The tungsten sulfide sample synthesized was characterized by XRD as WS_2 with a hexagonal structure (Figure S9). The morphology as visualized by SEM is shown in Figure S10.

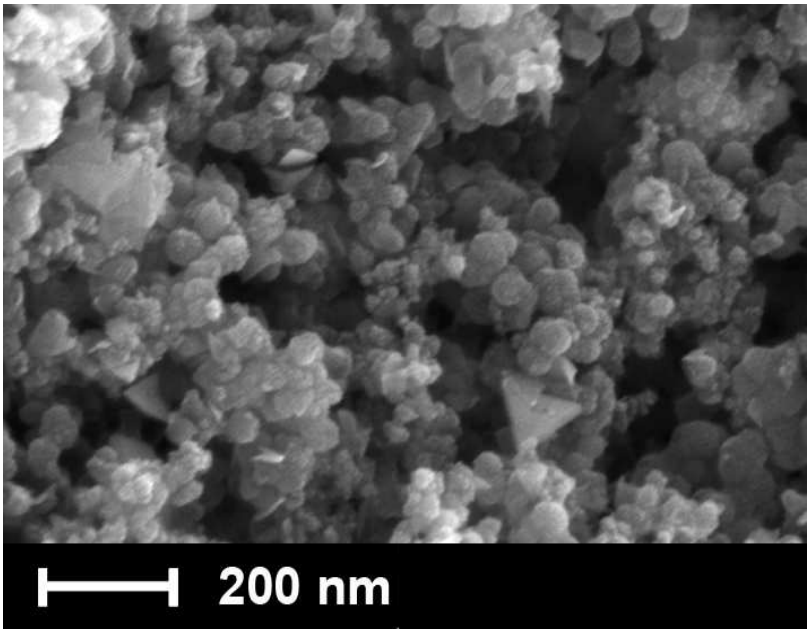

Figure S10. SEM image of tungsten sulfide supported on carbon. The triangular structure is seen for WS_2.

In the image, triangular crystallites are observed and are consistent with the known forms of WS_2. The atomic ratio of S to W measured by EDS (Table 1) is close to the stoichiometric composition for disulfides.

A Mo sulfide was synthesized and characterized by XRD (Figure S11) and TEM (Figure S12). The XRD spectrum had low-intensity peaks with a diffraction pattern that resembled the MoS_2 structure. The low degree of crystallinity was attributed to high dispersity of the nanometer size crystallites. The interlayer spacings of sulfide nanoparticles supported on graphite were determined by Fourier analysis on selected portions of TEM images (Figure S12). Regions with layered structure with spacing in the range 3.5–3.8 Å were identified as graphite structure (typical interlayer distances 3.4 Å) and the regions with layers spaced 5.6–6.4 Å apart were attributed to MoS_2 (typical interlayered spacing of 6.2 Å).

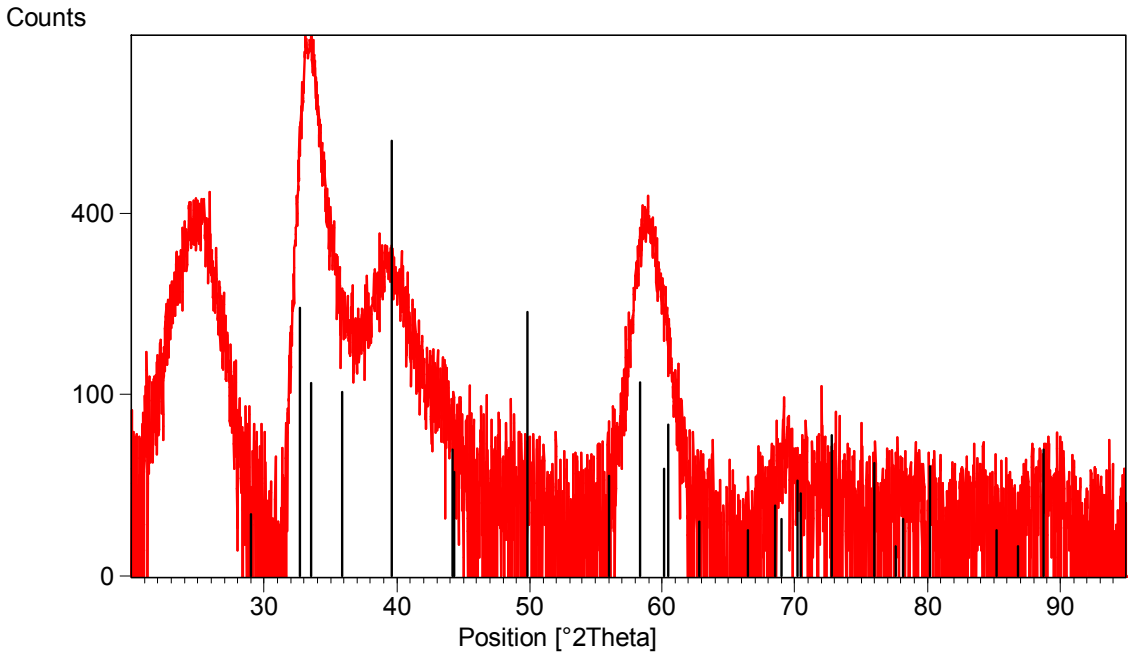

Figure S11. X-Ray Diffraction Spectrum of MoS_2

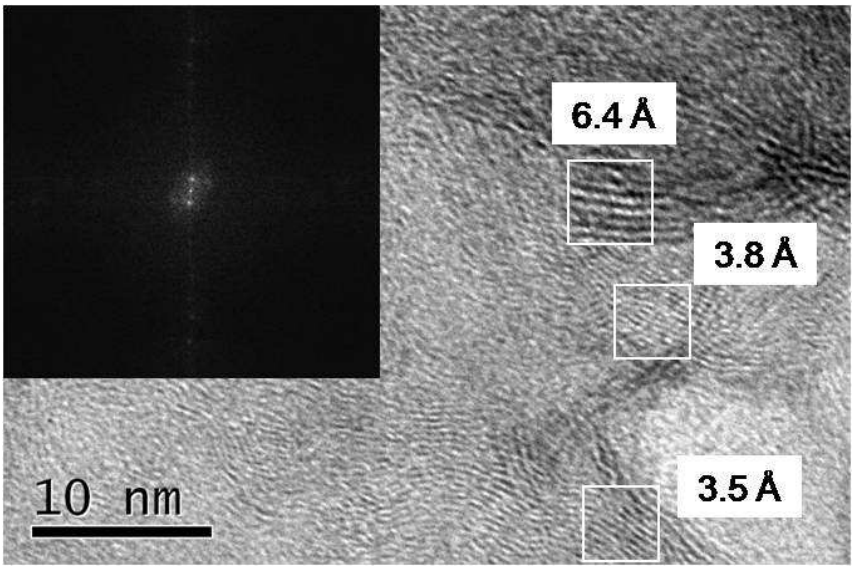

Figure S12. TEM image of Mo sulfide with Fourier transformation of the region with wide interlayer spacing. The white spot in the center of the inset image is the zero spot and the bright reflections correspond to the interlayer distance of 6.4 Å.

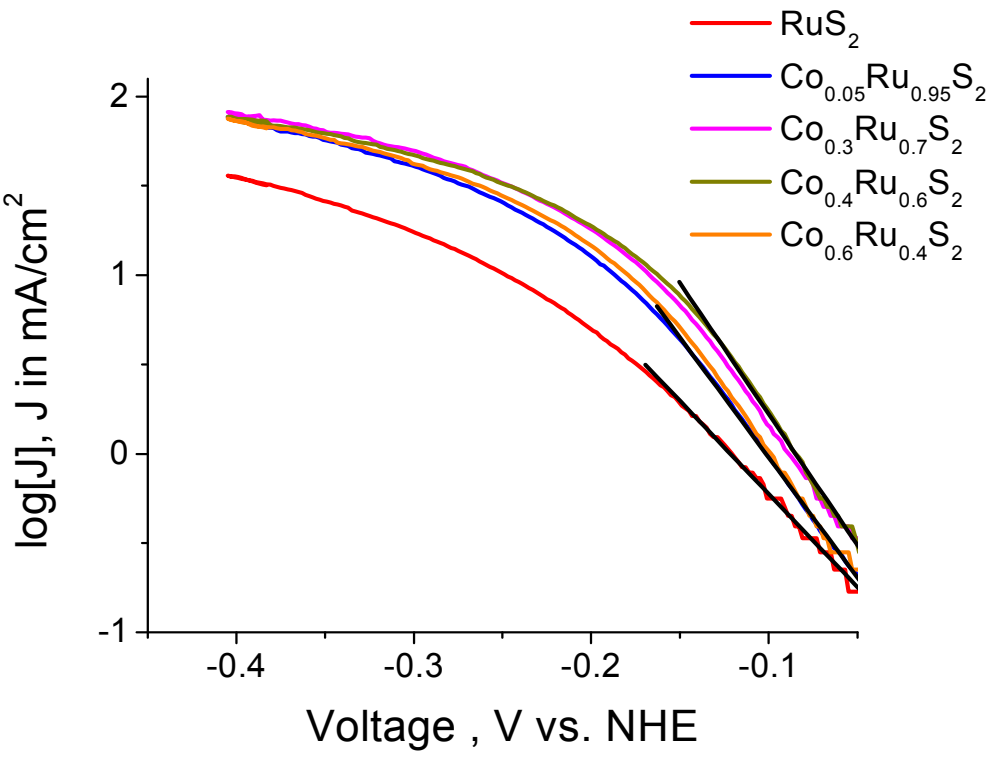

Figure S13. Cyclic voltammetry of Co-substituted RuS_2 catalysts with different cobalt substitution preparation concentrations with Tafel slopes (black lines). Electrolyte was 0.5M HBr and scan rate was 5 mV/second. The change in Tafel slope with substitution indicates a change shows the improvement in activity of RuS_2 through the substitution of cobalt.

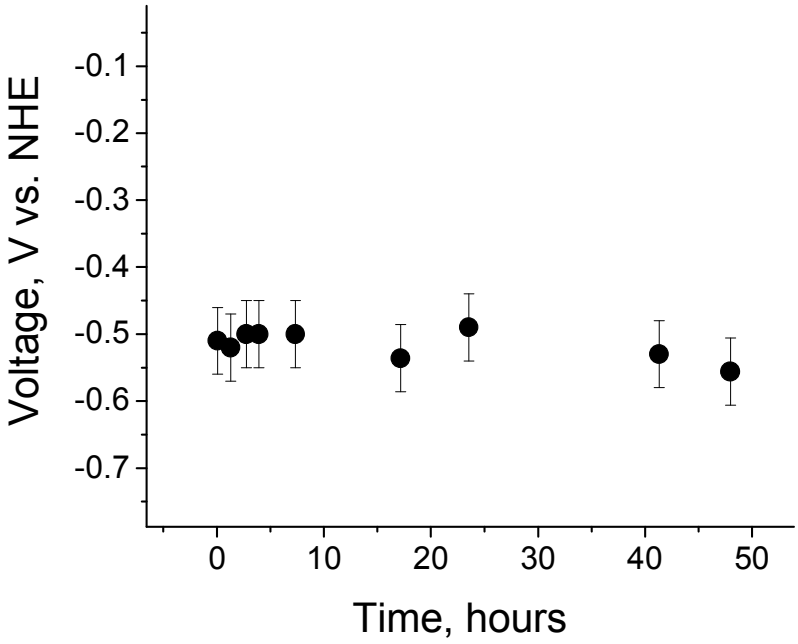

Figure S2. Chronopotentiogram for 100 mA/cm^2 during hydrogen evolution on 30% Co-substituted RuS_2 in 3M HBr.

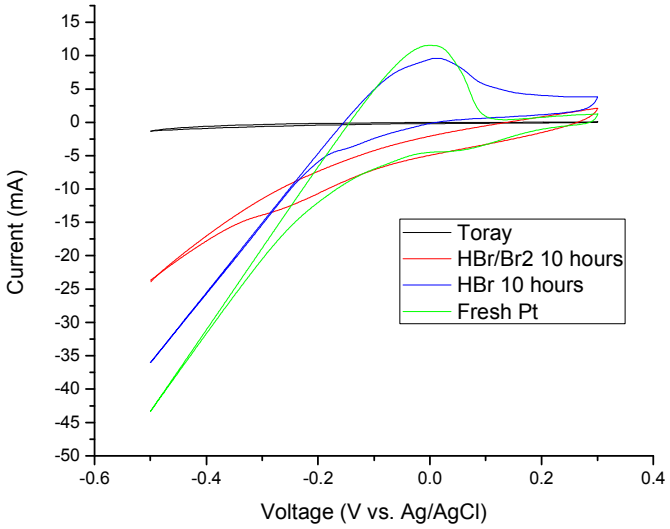

Figure S15. Decrease in hydrogen evolution activity from bromide/bromine poisoning of platinum electrode by being exposed to a solution of HBr or HBr/Br_2 for 10 hours. The Toray carbon substrate is also included for comparison. Scans were taken at a rate of 20 mV/second, the electrode was prepared on Toray paper with loading of 30 wt% Pt on carbon support

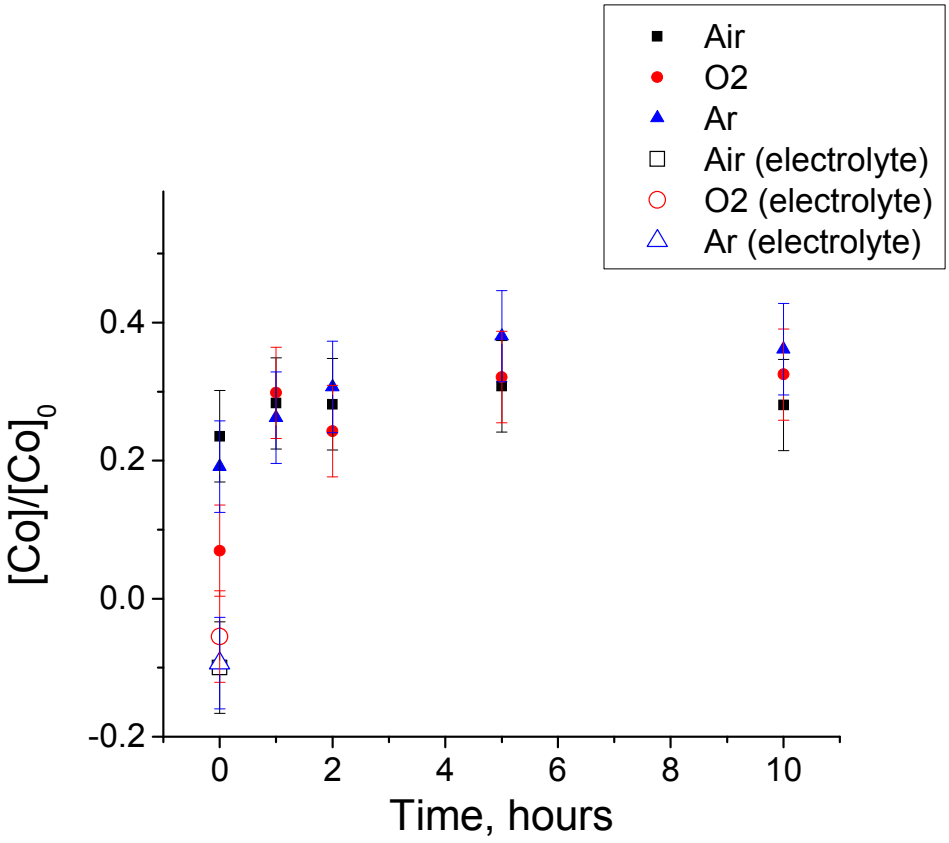

Figure S16. Co dissolution with time for different purge gases measured by ICP-AES

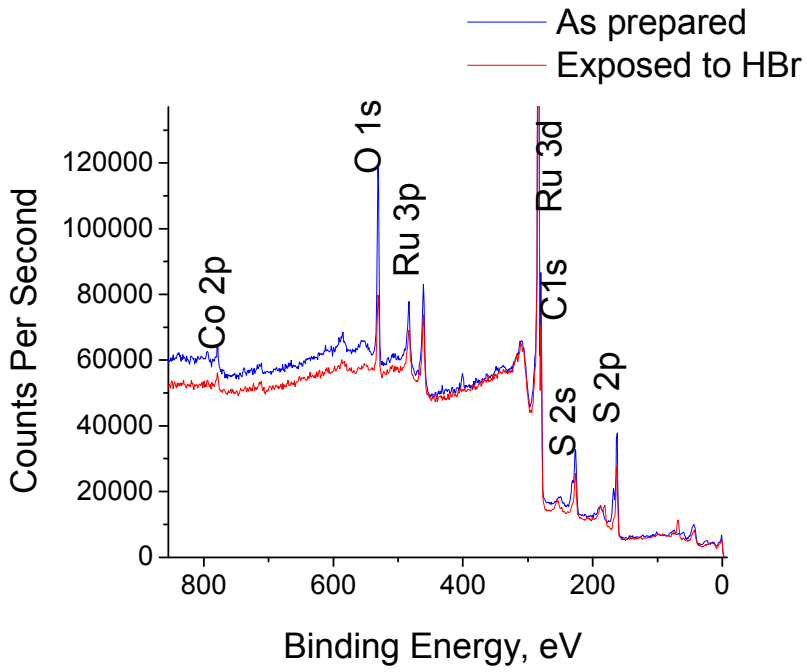

Figure S17. XPS survey scans of two 30% Co- substituted RuS_2 samples: freshly prepared and exposed to HBr.

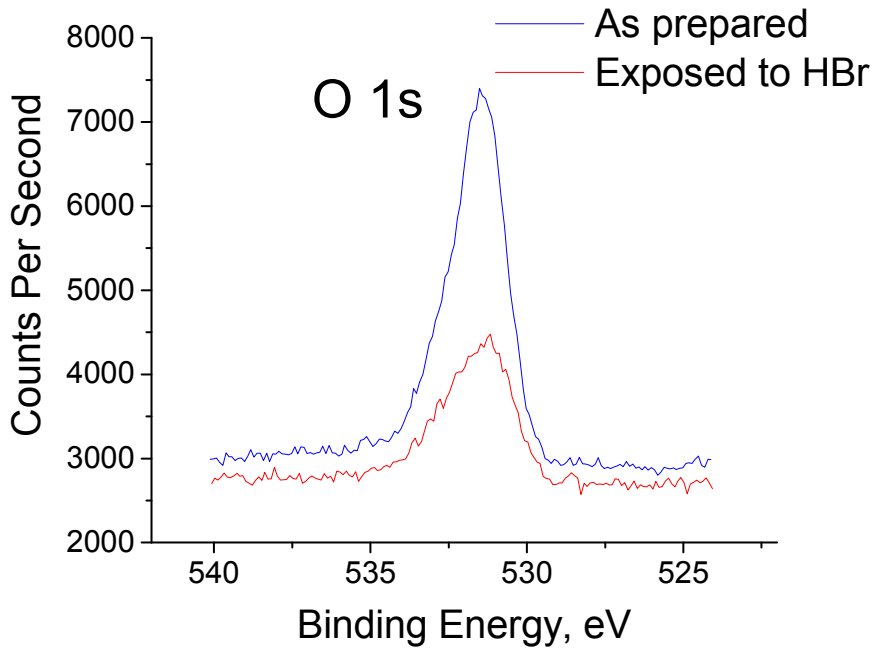

Figure S18. High resolution O 1s XPS spectra of two 30% Co- substituted RuS_2 samples: freshly prepared and exposed to HBr

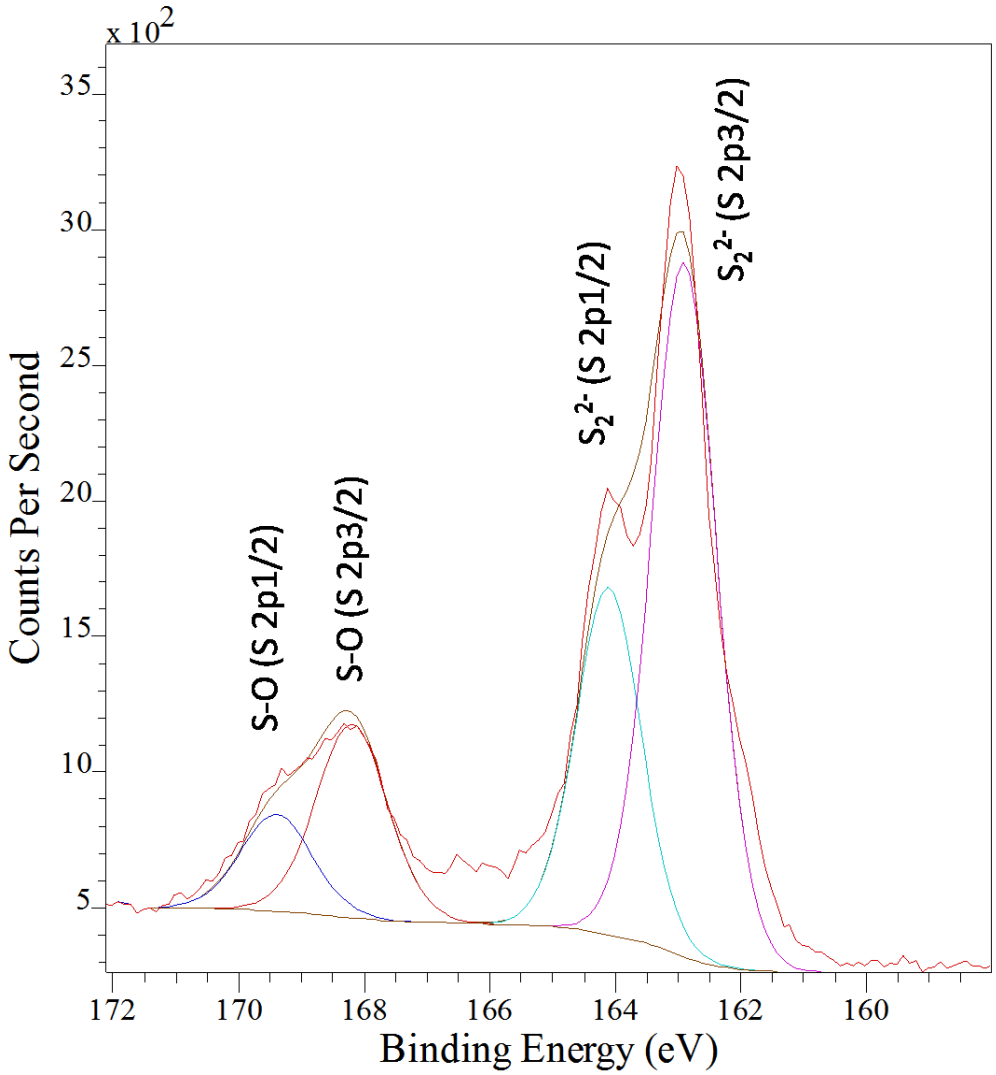

Figure S19. High resolution Sulfur 2p XPS spectrum of freshly prepared 30% Co-substituted RuS_2. The fitted peaks correspond to sulfur bound to metal (labeled as S_2^{2-}) and to oxygen (labeled as S-O)

Table S1. Atomic concentration (in percents of the total) of elements on the surface of freshly prepared and exposed to HBr 30% Co-substituted RuS_2 material on carbon (carbon excluded from quantification) obtained by XPS survey and high resolution S 2p spectra analysis

Sample	Co 2p3/2	Ru 3d3/2	O 1s	S 2p	S in S_2^{2-}, % of total S	S in S-O, % of total S
As prepared	2.0	11.6	38.1	48.3	76.7	23.3
Exposed to HBr	1.4	13.9	31.0	53.7	90.1	9.9

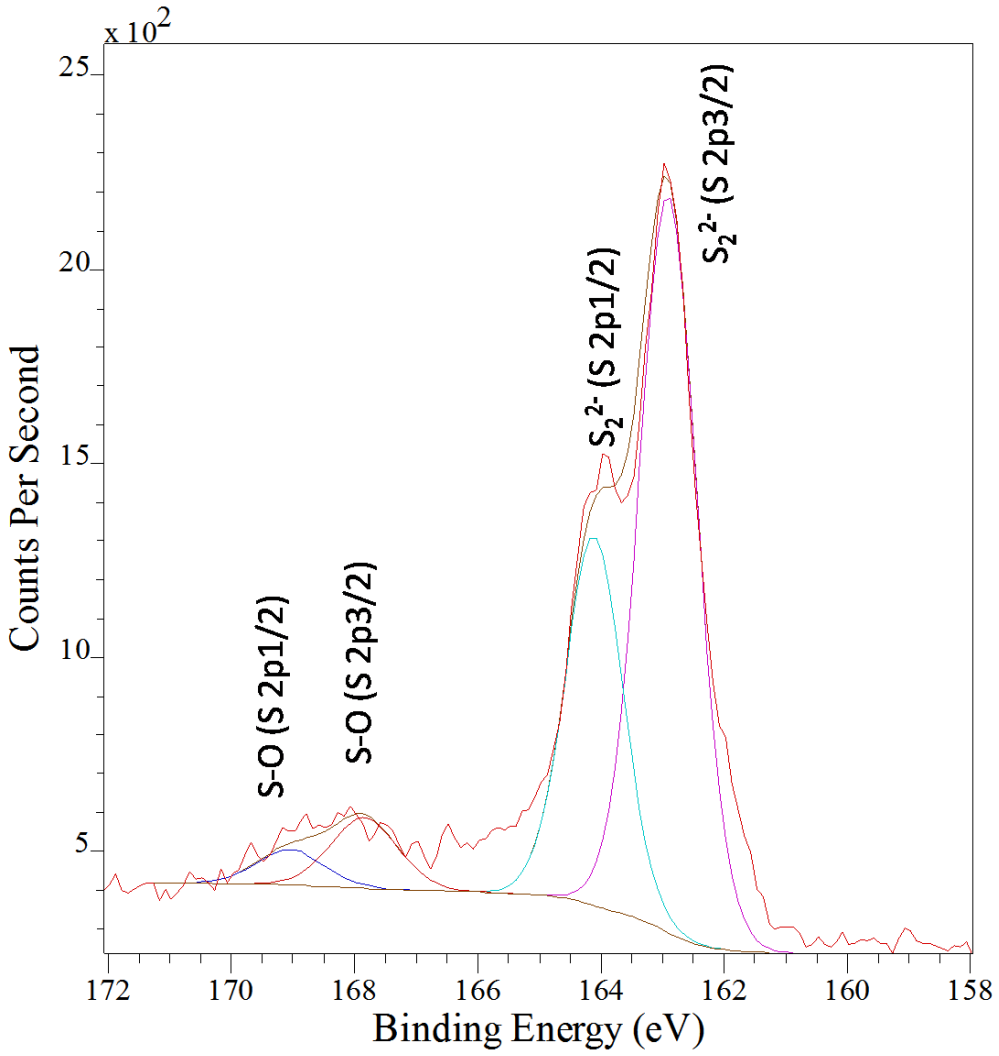

Figure S20. High resolution Sulfur 2p XPS spectrum of 30% Co-substituted RuS_2 sample after exposure to HBr. The fitted peaks correspond to sulfur bound to metal (labeled as S_2^{2-}) and to oxygen (labeled as S-O)

2) Calculations of the free energy of reaction

Since in the standard hydrogen electrode, the reaction

$$H_{2(g)} \leftrightarrow 2\left(H^+ + e^-(\text{SHE})\right) \tag{S1}$$

is always in equilibrium, at H_2 partial pressure of 1 bar, proton activity of 1, and T = 298K, the chemical potential of a proton in liquid phase is given by the chemical equilibrium condition[49, 50]

$$\mu^{\ominus}_{H^+}(T) = \frac{1}{2}\mu^0_{H_2}(T, 1\,\text{bar}) - \bar{\mu}_e(\text{SHE}). \tag{S2}$$

$\bar{\mu}_e(\text{SHE})$ is the electrochemical potential[50] of the standard hydrogen electrode. $\mu^0_{H_2}(T, 1\,\text{bar})$ is the chemical potential of gaseous H_2 when the pressure of hydrogen molecule equal to 1 bar and can be calculated by statistical mechanics:[49]

$$\mu^0_{H_2}(T, 1\,\text{bar}) = E(H_{2(g)}) + \mu^{t,0}_{H_2} + \mu^{vib}_{H_2} + \mu^{r}_{H_2} \tag{S3}$$

Here $E(H_{2(g)})$ is the binding energy of H_2. The translational contribution is $\mu^{t,0}_{H_2} = -RT\ln\left[\frac{RT}{1\,\text{bar}\,\Lambda^3}\right]$ with the de Broglie thermal wave length $\Lambda = \sqrt{\frac{h^2}{2\pi m_{H_2} k_B T}}$ at pressure of 1 bar. μ^{vib} and μ^{r} are the chemical potentials of vibration and rotation. The vibrational contribution consists mainly of the zero point energy.

For the hydrogen evolution reaction $2\left(H^+ + e^-(\text{W})\right) \rightarrow H_{2(g)}$, where W indicates the working electrode, we need to calculate the change in free energy for the reactions

$$* + \left(H^+ + e^-(\text{W})\right) \rightarrow H* \tag{S4}$$

and

$$H* + \left(H^+ + e^-(\text{W})\right) \rightarrow H_{2(g)} + * \tag{S5}$$

also taking place at the working electrode. Here * is an unoccupied surface site and H* is an adsorbed hydrogen atom. The free energy change for the reaction (S4), denoted by ΔG_{H*}^{Ads}, is given by

$$\Delta G_{H*}^{Ads} = \mu_{H*} - \mu_* - \left(\mu_{H^+}^{\ominus}(T) + RT\ln\left[a_{H^+}\right]\right) - \bar{\mu}_e(W) \qquad \text{(S6)}$$

Here μ_{H*} is the chemical potential of the hydrogen adsorbed on the RuS_2 slab and μ_* is the chemical potential of the slab without hydrogen. The latter is taken to be equal to the energy of the slab calculated by DFT. a_{H^+} is the proton activity in the working electrolyte. Using Equation S3 in Equation S6 gives

$$\Delta G_{H*}^{Ads} = \mu_{H*} - \mu_* - \left(\frac{1}{2}\mu_{H_2}^0(T, 1\text{ bar}) - \bar{\mu}_e(\text{SHE}) + RT\ln\left[a_{H^+}\right]\right) - \bar{\mu}_e(W) \qquad \text{(S7)}$$

The difference between the electrochemical potentials is relate to the voltage difference

$$\Delta U_{\text{SHE}} \equiv \left(\bar{\mu}_e(\text{SHE}) - \bar{\mu}_e(W)\right)/e \qquad \text{(S8)}$$

between the working electrode and the SHE. Here e is the electron charge.

The concentration of the electrolyte solution used in the present calculation is 0.5M HBr. The activity of this electrolyte is $a_{\text{HBr}} = \gamma_{\text{HBr}} m_{\text{HBr}} = a_{\text{H}^+} a_{\text{Br}^-}$; the activity coefficient[51] is $\gamma_{\text{HBr}} = 0.789$ and the concentration is $m = 0.5$. The mean ionic activity can be obtained from the relation[50, 51] $a_{\text{HBr}} = a_{\pm}^2$. Here we adapted $a_{\pm} \equiv a_{\text{H}^+}$ to represent the proton activity in the 0.5M HBr solution. We also use

$$\mu_{H*} - \mu_* = E(H*, \theta) - E(*) + \mu_{H*}^{vib} + RT\ln\left[\frac{\theta}{1-\theta}\right] \qquad \text{(S9)}$$

The term μ_{H*}^{vib} is the chemical potential due to the vibrations of the adsorbed hydrogen atom. The vibration perpendicular to the surface has a large frequency and only contributes the zero

point energy to the chemical potential; the other two vibrations ("parallel" to the surface) have low frequency and they contribute to both energy and entropy.

The logarithmic term arises from the fact that there are more adsorption sites than adsorbates. This formula ignores the contribution of the interactions between the adsorbed hydrogen atoms to the entropy but includes the interaction energy in the term *E(H*, θ)*.

Using Equations S3, S8, and S9 in Equation S7 gives

$$\begin{aligned}\Delta G_{H^*}^{Ads} &= \Delta E_{H^*}(\theta) + \mu_{H^*}^{vib} + RT\ln\left[\frac{\theta}{1-\theta}\right] \\ &\quad -\left(\frac{1}{2}(\mu_{H_2}^{t,0} + \mu_{H_2}^{vib} + \mu_{H_2}^{r}) + RT\ln\left[a_{H^+}\right]\right) + e\,\Delta U_{\mathrm{SHE}}\end{aligned} \tag{S10}$$

with

$$\Delta E_{H^*}(\theta) = E(H^*,\theta) - E(^*) - \frac{n}{2}E(H_2(g)) \tag{S11}$$

.

$E(H^*,\theta)$ is the energy of the surface with n hydrogen atoms adsorbed in the supercell, $E(^*)$ is the energy of the surface with no hydrogen, and $E(H_{2(g)})$ is the energy of a H_2 molecule in the gas phase; $\Delta E_{H^*}(\theta)$ is the adsorption energy of n hydrogen atoms leading to the coverage θ.

We used the calculated zero point energy for gaseous H_2, which is 0.287 eV per H_2. The activity of the HBr solution does not make a substantial difference in the change in the free energy. For HBr solutions in the concentration range of 0.5M HBr to 1M HBr, the change in the term $RT\ln[a_{H^+}]$ is of order of –0.02 eV.

For the desorption step in Equation S5, the change in free energy, denoted by $\Delta G_{H^*}^{Des}$, can be calculated by

$$\Delta G_{H^*}^{Des} = \mu_{H_2} + \mu_* - \mu_{H^*} - \left(\mu_{H^+}^{\ominus}(T) + RT\ln\left[a_{H^+}\right]\right) - \bar{\mu}_e(W) \tag{S12}$$

$$= (\mu_{H_2}^t + \mu_{H_2}^{vib} + \mu_{H_2}^r) - \frac{1}{2}\mu_{H_2}^{t,0} - \Delta E_{H^*}(\theta) - \mu_{H^*}^{vib}$$

$$-RT\ln\left[\frac{\theta}{1-\theta}\right] + e\Delta U_{\mathrm{SHE}} - RT\ln\left[a_{H^+}\right] \tag{S13}$$

where $\mu_{H_2}^t = \mu_{H_2}^{t,0}[T, 1\text{ bar}] + RT\ln\left[\frac{p_{H_2}}{1\,\mathrm{bar}}\right]$.

3) Cobalt dopant effect on the spatial dependence of adsorption energies ΔE_{H^*}

The DFT adsorption energy ΔE_{H^*} (Equation S11) of a hydrogen atom to a sulfur atom was calculated for two supercells. One supercell had the area $(\sqrt{6}\times\sqrt{2})a^2$ (a = 5.65 Å) and the surface layer contained 1 Co, 7 Ru, 14 sulfur atoms. The area of the other supercell was $(\sqrt{6}\times 2\sqrt{2})a^2$, its surface layer had 1 Co atom, 15 Ru atoms, and twice the number of sulfur atoms as the other. Increasing the size of the supercell lowers the H and Co concentration on the surface. The calculations were performed for one H atom per supercell. The values of ΔE_{H^*} for the two supercells are very close, indicating that in the small supercell there is no interaction between periodic images (decreasing Co and H concentration does not affect H binding energy to S). The adsorption energy depends on the distance of the S atom to the substituted Co but this dependence shows no clear trend. The site nearest to the substitution is hardly affected by its presence. However, the sites a bit further away bind H more strongly by about 0.1 eV. The calculations for the Co substitution on the M_{6c}^s site (see Figure 7b in the manuscript) give the same trends.

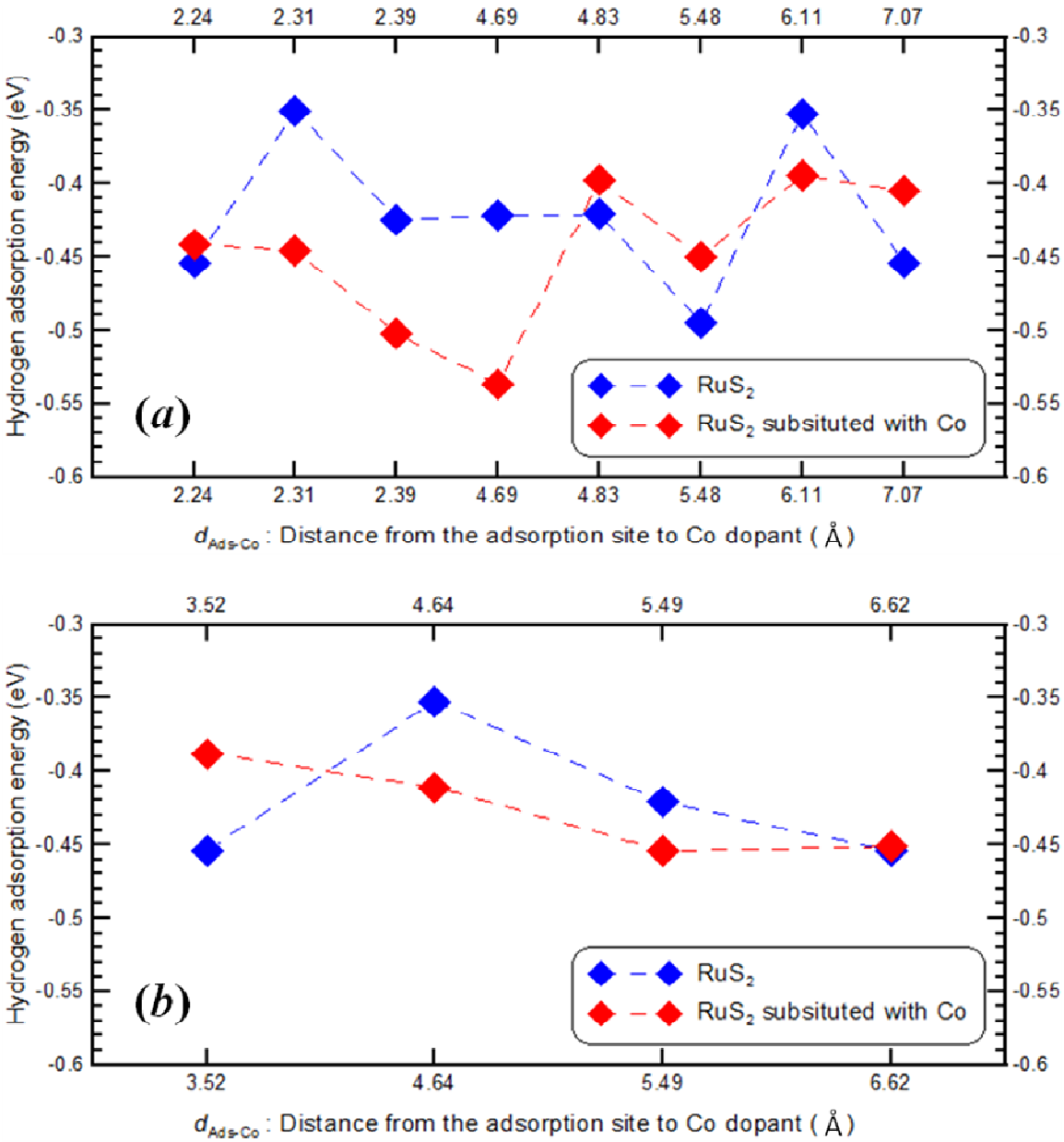

Figure S21. The adsorption energy ΔE_{H*} of one hydrogen atom on a S atom, as a function of the distance between the Co dopant and the adsorption site of H. The supercell size is such that the coverage of H atom is θ = 1/8. (a) The Co atom substitutes a Ru atom on the M_{6c}^{t} site (see Figure 7b in the $(111)_{S\text{-}S}$ surface model). There are two kinds of S atoms on the surface. The H located at 2.31 Å and at 6.11 Å from the Co atom is bound to SU_{3c} sulfur sites; the others are

bound to SP_{2c} sites; (b) The Co atom substitutes a Ru atom on the M_{6c}^{s} site. We show ΔE_{H*} on the undoped RuS_2 surface (blue) and the Co-substituted RuS_2 surface (red).